

# VALIDATION OF THE RADIOMETRIC PROCESSING CHAIN OF THE LEICA ADS40 AIRBORNE PHOTOGRAMMETRIC SENSOR

L. Markelin <sup>a,\*</sup>, E. Honkavaara <sup>a</sup>, U. Beisl <sup>b</sup>, I. Korpela <sup>c</sup>

<sup>a</sup> Finnish Geodetic Institute, Masala, Finland - (lauri.markelin, eija.honkavaara)@fgi.fi

<sup>b</sup> Leica Geosystems, Heerbrugg, Switzerland - ulrich.beisl@leica-geosystems.com

<sup>c</sup> Faculty of Agriculture and Forestry, P.O. Box 27, 00014, University of Helsinki - ilkka.korpela@helsinki.fi

**KEY WORDS:** Camera, Image, Radiometric, Calibration, Correction, Quality, Accuracy, Multispectral

## ABSTRACT:

Large-format photogrammetric digital airborne imaging sensors have been commercially available for several years. Their excellent radiometric properties compared to film-based imaging have been reported in several studies. Despite these radiometric advantages, up to now, airborne digital images have been exploited in a rather conventional manner in photogrammetric applications, even though methodologies from quantitative remote sensing, e.g. radiometric image correction and classification, could be utilized to raise the performance of photogrammetric applications to a new level. The recent state-of-the-art review revealed that the fundamental problem in the quantitative utilization of image radiometry in photogrammetric applications is the radiometric correction. Among digital photogrammetric large-format mapping sensors, the Airborne Digital Sensor (ADS) of Leica Geosystems is the only commercially available system at the moment having an integrated, physically based, radiometric correction chain. The processing does not require any in situ control information, as the radiometric corrections are based on *a priori* calibration information and image data. To validate performance of the processing chain, a comprehensive flight campaign was carried out with an ADS40 SH52 sensor in Finland in August 2008. We present the first results of the validation of the Leica ADS40 radiometric processing chain. The results indicated great performance potential. With the challenging data set, the differences of ADS40 and independent ground reference reflectance measurements were even less than 5% for uniform targets; atmospheric state, multispectral channel and flying height were detected as the major factors influencing the accuracy. Leica Geosystem's ADS40 can be considered as an efficient and accurate, 3D, multi-angular, multispectral imaging radiometer, which opens new interesting prospects for 3D remote sensing and characterization of the Earth surface. Results also indicated the importance of the test field validation process, gave improvement ideas for the sensor post-processing software and provided information for the development of validation methods.

## 1. INTRODUCTION

Digital imaging is replacing film imaging in photogrammetric data capture. In addition to the rigorous 3D-geometric performance, digital photogrammetric sensors offer excellent radiometric potential (Markelin et al., 2008).

A recent assessment of the state-of-the-art of radiometric processing in photogrammetric production lines of several European National Mapping Agencies showed that the radiometry is not processed quantitatively in operational processes (Honkavaara et al., 2009). Instead, radiometric processing is a complicated and laborious task, and the results are not typically satisfactory. The expected benefits of more accurate radiometric processing are the more automatic image processing, higher quality true-color and reflectance imagery, and better automation level of applications. Expected possibilities of the accurate, photogrammetric reflectance data are, for instance, reliable production of vegetation indices, utilization of spectral libraries, time series analyses, and enhanced change detection. In Finland an important prospect is the enhancement of the tree species classification, which is currently the bottleneck in automation of forest interpretation.

The requirements of quantitative radiometry have been taken into account in all aspects of the large-format photogrammetric mapping sensor of the Leica Geosystems, the Airborne Digital Sensor (ADS40, ADS80). The basis is an accurate, stable sensor, which performs radiance measurements in the blue (B), green (G), red (R) and near infrared (NIR) ranges of the

electromagnetic spectrum (Fricker, 2007). An important feature is the accurate radiometric laboratory calibration which is applied rigorously throughout the data processing (Beisl, 2006). The radiometry chain is completed by physically based radiometric correction methods, which are implemented in the ADS post-processing software, the Leica XPro (Beisl et al., 2008).

Leica Geosystems was the first photogrammetric sensor manufacturer to integrate quantitative processing of radiometry in the sensor post-processing line (Beisl, 2006; Beisl et al., 2008). Recently, also Intergraph has started improving the radiometric processing of the DMC (Ryan and Pagnutti, 2009). The practical experiences of XPro have indicated great improvements of processing efficiency, better radiometric homogeneity of the output image mosaics and improved performance e.g. in forestry applications (Beisl et al., 2008). However, thus far there exists no independent, quantitative assessment of the performance of the methodology.

The objective of this study was to validate the Leica ADS40/XPro at-sensor radiance and atmospherically corrected ground reflectance products. We also considered radiometric validation aspects of airborne sensors. The study was performed using ADS40 data from a comprehensive empirical flight campaign carried out in Finland in August 2008. The image data set is one of the image materials offered in the context of the European Spatial Data Research (EuroSDR) research

\* Corresponding author.

project “Radiometric aspects of digital photogrammetric airborne images” (Honkavaara et al., 2009).

## 2. MATERIALS AND METHODS

### 2.1 The Leica ADS40 sensor and the XPro radiometric processing chain

The ADS40 is a large-format photogrammetric sensor based on the pushbroom principle. In this study the sensor head 52 (SH52) is used which has a total of 12 CCD-lines installed in different positions on the focal plane to provide different along track viewing angles: nadir panchromatic (PAN; 2°), nadir R, G, B and NIR (0°), backward PAN (14°), backward R, G, B and NIR (16°) and forward PAN (27°) (Fricker, 2007).

The manufacturer performs comprehensive absolute radiometric calibration for the ADS, including corrections for dark signal non-uniformity (DSNU), photo response non-uniformity (PRNU), absolute radiometric response, and spectral response (Beisl, 2006). Since the sensor response w.r.t. incident radiance data and integration time is linear, the radiometric model for retrieving the at-sensor radiance from raw digital numbers (DN) for a specific multispectral (MS) channel is given by:

$$CDN = DN * 50 * c_1 / IT \quad (1)$$

where CDN is calibrated DN (16 bit integer), DN is recorded raw DN (16 bit integer),  $c_1$  is radiometric gain (camera and channel specific), IT is integration time (s) and 50 is scale factor.

CDN data are stored as epipolar rectified 16 bit integer images. The band-averaged spectral radiance  $L$  [ $W/(m^2 \text{ sr } \mu\text{m})$ ] of the band is calculated by dividing the CDN with the scale factor 50.

Leica XPro is used for the entire post-processing workflow of the ADS-imagery from data download to the generation of stereo models and orthoimages. In radiometric terms, main features are the options to produce radiometrically corrected ground radiance and ground reflectance images. The default product of XPro is calibrated DN (equation 1), which relates the pixel data to at-sensor radiances. There are two options to produce ground radiance data: the Dark Pixel Subtraction (Chavez, 1975) and the Modified Chavez (Chavez, 1988) methods. Ground radiances are still dependent on the illumination level and vary from flight line to flight line. To overcome this, there is an option for atmospheric correction and reflectance calibration based on the radiative transfer equation by Fraser et al. (1992) and a parameterization of the atmospheric parameters based on the method of Song et al. (2003). This atmospheric correction results in images where the DNs are calibrated to ground reflectances. In ground reflectances, the reflected radiance is divided by the incoming solar irradiance which results in a surface property. All three correction methods are based on an automatic dark object method to tune the corrections to the actual atmospheric conditions. Additionally, BRDF (Bidirectional reflectance distribution function) correction based on a modified Walthall model is implemented in XPro. The details of the correction methods are in Beisl et al. (2008). All corrections rely entirely on *a priori* calibration information and atmospheric information derived from dark pixels in the image data.

### 2.2 Imagery

A flight campaign was carried out at the Hyytiälä forestry research station in Finland (62°N, 24°E) on 23 August, 2008 using a Leica ADS40 SH52 digital photogrammetric camera to validate the sensor performance and to evaluate data performance in forestry applications. A total of 15 flight lines were collected from four flying heights (1, 2, 3 and 4 km, resulting ground sampling distances (GSDs) 10, 20, 30 and 40 cm, respectively) of which 4 were used here. The MS channels (R, G, B, NIR, both nadir and backward directions) were recorded in raw (uncompressed) mode. The weather conditions were mostly clear, but some small clouds were over the area. The detailed information of the images used and atmospheric conditions are in Table 1.

Flying height	1km	2km	3km	4km
GSD [cm]	10	20	30	40
Flying direction	349°	349°	349°	169°
Integration time [ms]	1.94	2.77	4.16	5.54
Off-nadir viewing angle	15°	3.5°	3.2°	10.7°
Start time (UTC+3)	10:25	10:45	11:18	11:43
End time (UTC+3)	10:28	10:48	11:20	11:47
Sun elevation angle	30.0°	31.8°	34.5°	36.2°
Sun azimuth angle	126.6°	131.9°	141°	148.3°
Visibility [km]	49.6	42.8	50.0	50.0
Temperature [°C]	14.6	14.9	15.0	15.5
AOT 500nm	0.16	0.15	0.17	0.16
CO2 [ppm]	373	372	374	372
O3 [g/cm2]	6.54E-04	6.54E-04	6.54E-04	6.54E-04
H2O [g/cm2]	1.41	1.40	1.45	1.39

Table 1. Information of image lines used and weather conditions.

**2.2.1 Image processing:** The nadir-looking MS (R, G, B, NIR) image lines were used, one from each flying height. Two versions of each image were produced using XPro version 4.1:

- No corrections (ASR, at-sensor radiance data)
- Atmospheric (ATM, ground reflectance data)

The ASR-data enables the evaluations of vicarious calibration and the ATM-data is, according to user experiences, the most useful radiometrically corrected product. The BRDF-correction was not tested in this study, because an improved method with water masking will be implemented in the XPro version 4.2.

The images were processed into small patches that covered the ground reference targets (section 2.3, Figure 3). For each target and MS channel the average, minimum, maximum and standard deviation of at-sensor radiances and ground reflectance were calculated in image windows of ground size of 3 m x 3 m.

### 2.3 In situ measurements

The radiometric reflectance targets included four portable reference reflectance targets (tarps) of the Finnish Geodetic Institute (FGI) (Markelin et al., 2008) installed on the grass football field and various natural and manmade covers (Figure 3, Table 2). During the campaign the nadir spectra of the reference targets were measured using an ASD Field Spec Pro FR spectroradiometer. 12–20 spectra were measured over each target and then averaged to get the final spectra. Before and after each target measurement a reference measurement was made with a calibrated white reference standard (12" Spectralon from Labsphere). The spectra were measured in absolute radiance mode. Afterwards the radiances were scaled with the white reference measurements to produce target reflectances.

Finally, the target reflectances were weighted with the ADS40 channel spectral sensitivities to get the reflectances per MS channel (Figure 4).

The average measurement accuracy of the reference was estimated to be better than 6% for uniform targets and between 6–20% for other targets (Table 2). In the ADS40 data the cross-track viewing angles of the reflectance targets were 3–15°; the viewing angle in along-track direction was close to zero. The reflectance anisotropy of the reference tarps was analyzed in the laboratory. Tarp P05 with the 10 cm data viewing angles had the highest differences from the nadir reflectance; the difference was 5–10% depending on the channel; differences were 0–5% for other GSDs and targets. Therefore the tarp P05 was not used in the context of the data with the 10 cm GSD.

The Hyttiälä forest research station is equipped with the state-of-the-art SMEAR-II weather station (SMEAR, 2009), which is also part of the NASA AERONET network (Holben et al., 1998). The station provides continuously information about the atmospheric conditions which can be used in radiative transfer calculations.

SH	Target	Time	Sun El.	Sun Az.	Refl.	CV%
A	asphalt	9:59	27.4	120.0	0.140	2.8
B	grass1	10:08	28.4	122.2	0.078	4.9
C	grass2	10:16	29.1	124.3	0.068	9.6
E	sand	10:44	31.7	131.6	0.187	21.0
F	gray gravel1	10:54	32.6	134.4	0.090	8.7
G	gray gravel2	11:00	33.1	136.0	0.090	8.3
H	weeds1	11:09	33.8	138.5	0.100	21.3
I	weeds2	11:14	34.2	139.9	0.062	22.0
P05	tarpaulin 05	10:21	29.6	125.6	0.057	4.9
P20	tarpaulin 20	10:25	30.0	126.6	0.181	2.8
P30	tarpaulin 30	10:29	30.4	127.7	0.261	5.6
P50	tarpaulin 50	10:33	30.8	128.7	0.442	2.9

Table 2. Ground reference targets. SH = short name for target, Time = measurement time (UTC+3), Sun El. = Sun elevation, Sun Az. = Sun azimuth angle (0 = north), Refl. = average target reflectance on green channel (550nm), CV% = ground measurement Coefficient of Variation (100\*stdev/mean) for green channel.



Figure 3. Ground reference targets with identifiers in Table 2.

## 2.4 Validation

**2.4.1 The accuracy assessment.** The accuracy was assessed by using the ASD reflectance measurements as the reference (absolute accuracy) and by using the imagery with 10 cm GSD as the reference (comparisons of different flying heights). The reflectance differences were normalized with the reference reflectance:

$$Difference = 100 * (ATM\_data - reference) / reference \quad [\%] \quad (2)$$

This data was calculated for each target, flying height and MS channel. The more detailed analysis was performed using the accurate reference reflectance targets. The root-mean-squared (RMS) values of the differences were calculated for each flying height and channel.

$$RMS = \sqrt{\frac{\sum_{i=1}^n Difference^2}{n}} \quad [\%] \quad (3)$$

where  $n$  is number of targets used in the evaluation. The number of targets was four excluding the data with 10 cm GSD where the P05 was not used due to anisotropy effects (Section 2.3)

**2.4.2 Vicarious calibration.** The vicarious calibration was performed using simulated at-sensor radiances and ADS40 raw DN's (equation 1) of the four reference reflectance tarps (three tarps for 10 cm data). A linear regression was used to determine the gain and offset parameters. Details of the method are presented in Markelin et al. (2008). The differences of the gain parameters determined by the vicarious and the laboratory calibration were then calculated. Furthermore, the differences between the ADS40 and simulated at-sensor radiances were calculated using equation (2).

The simulated at-sensor radiances were calculated by the MODO software (ver. 3.0.9, based on a MODTRAN4 ver. 3.1 radiative transfer code) using the ground reflectance measurements and the atmospheric measurements of the SMEAR-II and AERONET stations. The parameters used in the simulations were flying height, solar angles, and the following atmospheric parameters from SMEAR-II: temperature, visibility and CO<sub>2</sub>, and from AERONET: H<sub>2</sub>O and O<sub>3</sub> (Table 1). A "Midlatitude summer" atmospheric model was used in the simulations. Also the aerosol optical thickness (AOT) at 500 nm from AERONET was observed as an indicator of the general conditions. The effects of aerosol measurement accuracies were not considered in this study.

## 3. RESULTS AND DISCUSSION

### 3.1 Validation of XPro-reflectance products

The general view of the reflectance data is shown in Figure 4. The reflectance of grass, asphalt and two reflectance targets (P20 and P50) measured in field and by ADS40 are shown. All measurements showed similar patterns but also differences appeared.

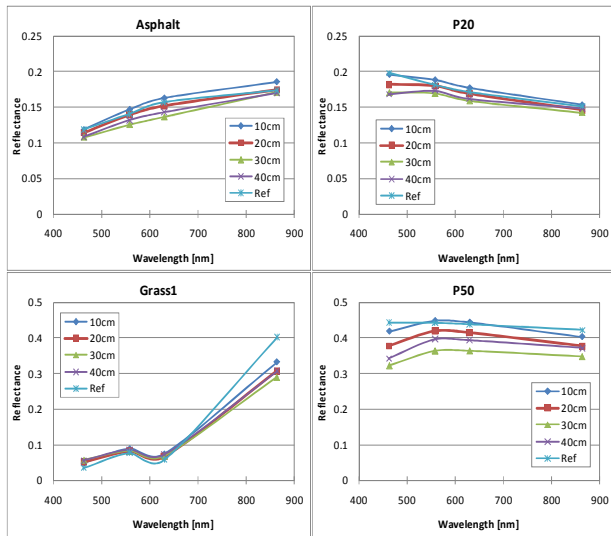


Figure 4. Reflectance of grass and asphalt targets, and two tarps (P20, P50) obtained from atmospherically corrected images and by ASD field measurements (Ref).

**3.1.1 Absolute reflectance accuracy.** The absolute accuracy was assessed by calculating the differences between the ADS40 reflectance data and the ASD field measurements. Differences (% of reflectance) of individual targets (10 cm and 40 cm data) and RMS-values of differences on reference reflectance tarps are shown in Figure 5a.

The differences on individual objects were in many cases substantially large, varying between 0–70%. The largest differences appeared on spatially non-uniform targets (grass, weeds); for uniform targets (asphalt, sand, reflectance tarps) the differences were less than 20%. Various channels provided different results; the differences were typically the largest in the B channel and the smallest in the R channel. The general performance of the 20 cm and 30 cm GSDs was similar to the 10 cm and 40 cm GSDs. However, the differences appeared to increase with increasing flying height. Furthermore, the performance of data with 30 cm GSD was clearly the worst, because there were some clouds close to the reflectance targets. The above observations indicated that the larger the influences of the atmosphere were, the poorer the absolute accuracy was.

Further analysis was performed using the reflectance tarps. The R, G and NIR channels provided in most cases differences lower than 10%, and in best cases differences lower than 5%

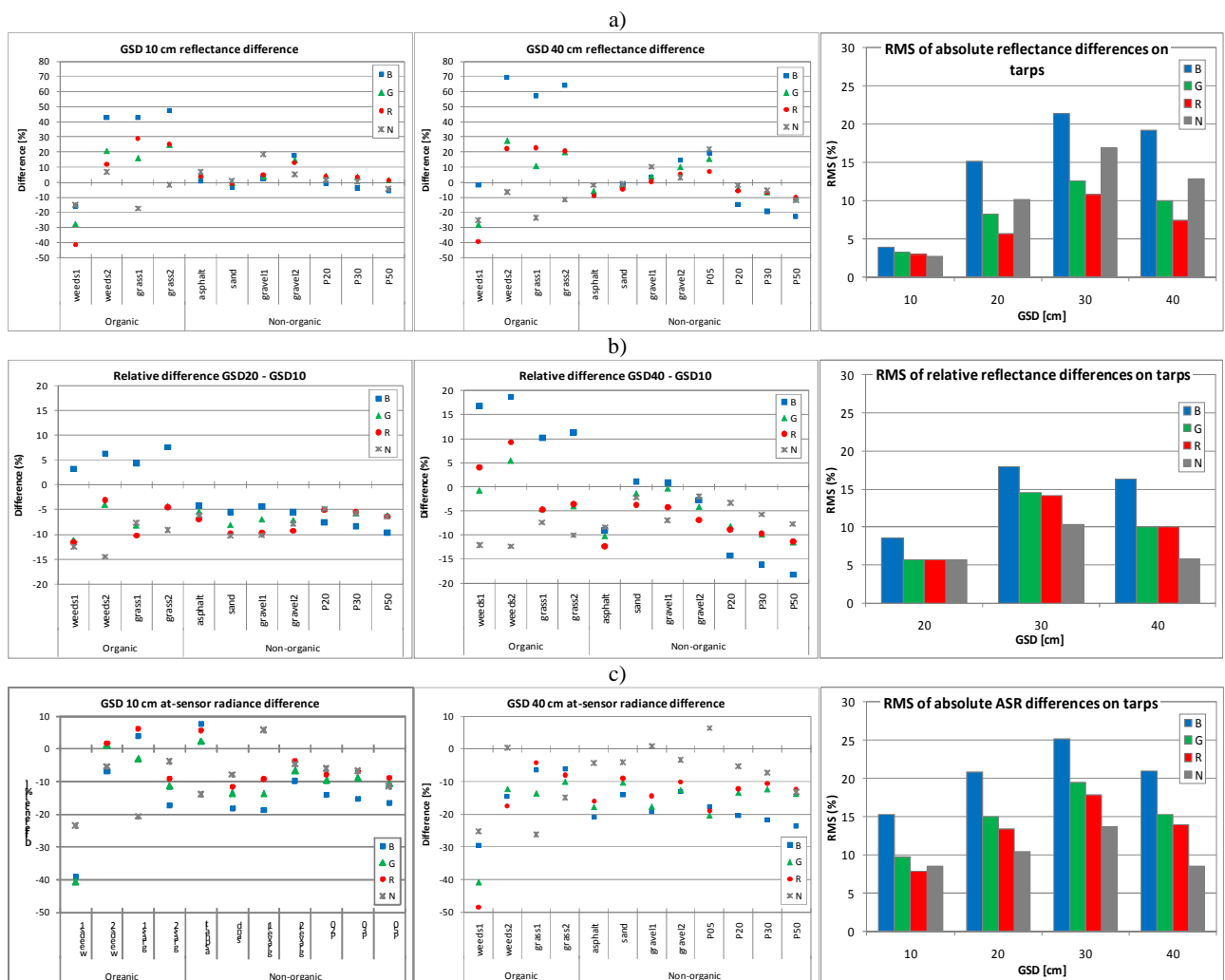


Figure 5 a) Absolute reflectance differences (%) for different objects: GSD 10 cm (left) and 40 cm (middle) and RMS of absolute differences on tarps (right). b) Comparison of different flying heights: GSD 20 cm (left) and GSD 40 cm (middle) and RMS of relative differences on three tarps (right). The image with 10 cm was used as a reference. c) Absolute at-sensor radiance differences (%) for different objects: GSD 10 cm (left) and 40 cm (middle) and RMS of absolute differences on tarps (right).

(Figure 5a). The RMS values of differences are given in Figure 5a (right). With 10 cm data the RMS values were less than 5%. The RMS values of the R channel were 5% or lower on 10 cm and 20 cm data. With 10, 20 and 40 cm data, in most cases, the RMS values were lower than 10%. In the case of the B channel the RMS values were up to 20%.

An unexpected phenomenon was that the differences normalized by the reflectance were dependent on the magnitude of the reflectance. Systematic features in Figure 5a indicated this. As an example, the differences of most uniform objects (tarps, asphalt, sand, gravel) are plotted as a function of the reflectance (NIR-channel) in Figure 6. In this case the systematic features were modeled with a linear regression; the coefficients of determination ( $R^2$ ) rose up to 0.7. The systematic trend was higher for the NIR and B channels than for the R and G channels, and it increased with the flying height.

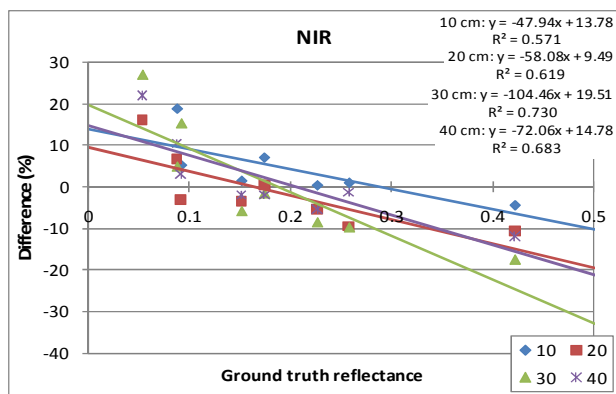


Figure 6. Absolute reflectance difference (%) of the NIR-channel as a function of the reflectance.

**3.1.2 Comparisons between different flying heights.** The relative accuracy of 20 cm, 30 cm and 40 cm data was assessed by using the 10 cm data as a reference; differences of individual targets and RMS values of differences for the reflectance tarps are given in Figure 5b.

The differences between the flying heights were lower than absolute differences, but similar features appeared in both cases (Section 3.1.1). The relative differences on various objects were 0–20%. The differences on reflectance tarps were mostly less than 10% for images with 20 and 40 cm GSD (excluding B channel) (Figure 5b). The RMS values of the NIR, R and G channels were 5–10% for GSDs 20 cm and 40 cm; RMS values of 30 cm data were 10–18% (Figure 5b, right). The individual channels provided different results. As with the absolute differences, differences were the largest on the B channel.

Again, the differences appeared to be systematically dependent on the magnitude of the reflectance. As in the case of absolute differences, the systematics was the highest on B and NIR channels and 30 cm and 40 cm data.

### 3.2 Evaluation of vicarious calibration

The differences of ADS40 and simulated at-sensor radiances are shown in Figure 5c. The differences are systematically negative, indicating that the simulation provided too high at-sensor radiance values. The RMS values in Figure 5c (right) are higher than the RMS values of the absolute reflectance differences of XPro ATM-data (Figure 5a (right)), except for the NIR channel; XPro provided thus better results in most cases. Similar,

radiance level dependent, systematic differences appeared on the at-sensor radiances derived by MODTRAN4 and the ADS40 as with the relative and absolute analysis of the reflectance data.

The vicarious calibration was compared to the laboratory calibration and differences of gain parameters were calculated. As could be expected based on the systematic difference of the ADS40 and simulated at-sensor radiance (Figure 5c), there was a substantially large difference between the vicarious calibration and laboratory calibration. The differences were the smallest in the R and G channels; for the 10 cm GSD the difference was 10% and for 20 cm and 40 cm GSD the difference was 10–15%. The differences were larger on B and NIR channels and they appeared to increase with the flying altitude. The above results indicated that the simulated at-sensor radiances based on MODTRAN4 radiative transfer code did not perfectly fit the data. However, the weather conditions were not optimal for the vicarious calibration.

### 3.3 Discussion

The preliminary results of the performance evaluation of the ADS40/XPro at-sensor radiance and atmospherically corrected reflectance products were given here.

The weather conditions were not perfect. The visibility was good, but the clouds changed the diffuse illumination. The conditions were typical of Finland, thus the results are representative in Finland. We feel that it is important to evaluate the performance also in suboptimal conditions.

The flying height influenced the accuracy. The difference between the ADS40 reflectances and the reference measurements increased for denser atmosphere, i.e. for higher flying heights. The results showed differences of 5% or even lower between the ADS40 and the field reference measurements for the 1 km flying height and uniform reference targets. For the 4 km flying height, as low as 10% differences could be obtained. Clouds caused further challenges for the radiometric corrections. These issues could be considered in future developments of the correction software.

Performance varied between the MS channels. The R channel appeared to be the most accurate with 5–7% absolute RMS values in up to 4 km flying height, and the performance of the G channel was very similar. The accuracy of NIR channel was lower than that of the R and G channels (7–12% absolute RMS values) and the B channel was the poorest (up to 20% RMS values). The results suggested a general undercorrection of the atmospheric effects.

The differences between ADS40 and field reflectance measurements were dependent on the target. The tarps, which are spatially uniform targets with low anisotropy, provided lower differences than the structural, natural objects. This can be attributed to the fact that the 1 mrad instantaneous field of view (IFOV) of the ADS40 pixel differs strongly from the 52 mrad IFOV of the ASD spectrometer. BRDF effects from different FOV and different diffuse illumination will result in different reflectances. Also natural vegetated surfaces (e.g. grass and weeds) are difficult to use as reference targets because of strong BRDF effects and changes of moisture during the day. Spatially uniform and temporally stable targets are highly recommended for calibration and validation purposes.

An important observation was that the difference normalized by the reflectance was dependent on the magnitude of the reflectance; more uniform performance would have been expected. This behavior appeared in comparisons of ADS40 and field reference measurements, comparisons between different ADS40 GSDs, and comparisons of MODTRAN4 and XPro derived at-sensor radiances. This result indicated that the atmospheric modeling was not quite accurate in either case to fit the actual atmospheric conditions.

The results from the quantitative performance evaluation of the ADS40 image processing chain could be considered as very good. The processing chain was also very efficient from the operational point of view. The radiometric processing was simple and automated; the user did not have to set any parameters. The corrections were based solely on the image data, thus the processing did not require any field reference targets. For the cases where reflectance targets are available, a recommended improvement for the software would be to enable their use.

The results indicated the importance of the radiometric test field validation. They showed quantitatively the high performance potential of the ADS40 radiometric processing chain and also identified improvement proposals. For the validation process it appeared to be advantageous to apply four calibration targets, distributed on reflectance range of 0.05–0.5.

In our future studies we will further evaluate the performance of the BRDF correction of the XPro software and also evaluate the spectro-directional performance of the system by analyzing the off-nadir views. An important future objective will be to evaluate the performance of the ADS40 imagery in the classification of tree species in Finland.

#### 4. CONCLUSIONS

This article provided preliminary results of the validation of the ADS40 radiometric processing chain. The results indicated that for the current algorithm and the evaluated challenging data set, up to 5% reflectance accuracy could be obtained for uniform targets. The accuracy was influenced by the flying height (1–4 km), channel (R, G, B, NIR), level of cloudiness and target properties. Considering that this was the first, independent quantitative assessment of the absolute accuracy of the ADS40/XPro reflectance products, the results can be considered as very promising. The study also pointed out improvement proposals for the correction method and the validation process.

It can be expected that the future of radiometrically quantitative photogrammetry is bright. On the way towards quantitative radiometric processing chains, the radiometric validations are crucial.

#### REFERENCES

- Beisl, U., 2006. Absolute spectroradiometric calibration of the ADS40 Sensor. In: *The International Archives of the Photogrammetry, Remote Sensing and Spatial Information Sciences*, Paris, France, Vol. XXXVI, part 2.
- Beisl, U., Telaar, J., and Schönemark, M. V., 2008. Atmospheric correction, reflectance calibration and BRDF correction for ADS40 image data. In: *The International Archives of the Photogrammetry, Remote Sensing and Spatial Information Sciences*, Beijing, China, Vol. XXXVII, part B7.
- Chavez, P. S., Jr., 1975. Atmospheric, solar, and MTF corrections for ERTS digital imagery. Proc. Am. Soc. Photogrammetry, Fall Technical Meeting, Phoenix, AZ, p. 69.
- Chavez, P. S., Jr., 1988. An improved dark-object subtraction technique for atmospheric scattering correction of multispectral data. *Remote Sensing of Environment*, 24(3), pp. 459-479.
- Fraser, R. S., Ferrare, R. A., Kaufman, Y. J., Markham, B. L., and Mattoo, S., 1992. Algorithm for atmospheric corrections of aircraft and satellite imagery. *International Journal of Remote Sensing*, 13(3), pp. 541-557.
- Fricker, P. Raising the bar for multi-band, high-resolution airborne imagery, 2007. In *Photogrammetric Week '07*; Fritsch, D., Ed.; Wichmann Verlag: Heidelberg, Germany, 2007; pp. 71-79.
- Honkavaara, E., Arbiol, R., Markelin, L., Martinez, L., Cramer, M., Bovet, S., Chandelier, L., Ilves, R., Klonus, S., Marshal, P., Schläpfer, D., Tabor, M., Thom, C., and Veje, N., 2009. Digital airborne photogrammetry — A new tool for quantitative remote sensing?—A state-of-the-Art review on radiometric aspects of digital photogrammetric images. *Remote Sensing* 1(3), pp. 577-605.
- Holben, B.N., Eck, T.F., Slutsker, I., Tanré, D., Buis, J. P., Setzer, A., Vermote, E., Reagan, J.A., Kaufman, Y.J., Nakajima, T., Lavenu, F., Jankowiak, I., and Smirnov, A., 1998. AERONET—A federated instrument network and data archive for aerosol characterization. *Remote Sensing of Environment* 66(1), pp. 1–16.
- Markelin, L., Honkavaara, E., Peltoniemi, J., Ahokas, E., Kuittinen, R., Hyypä, J., Suomalainen, J., and Kukko, A., 2008. Radiometric calibration and characterization of large-format digital photogrammetric sensors in a test field. *Photogrammetric Engineering & Remote Sensing* 74 (12), pp. 1487-1500.
- Ryan, R. E., and Pagnutti, M., 2009. Enhanced absolute and relative radiometric calibration for digital aerial cameras. *Proceedings of the Photogrammetric Week 2009*, Stuttgart, Germany.
- SMEAR, 2009. Smear research stations. <http://www.atm.helsinki.fi/SMEAR/> (Accessed 23 Nov. 2009)
- Song, J., Lu, D., and Weseley, M. L., 2003. A simplified atmospheric correction procedure for the normalized difference vegetation index. *Photogrammetric Engineering and Remote Sensing*, 69(5), pp. 521-528.

#### ACKNOWLEDGEMENTS

The financial support of the Ministry of Agriculture and Forestry of Finland is gratefully acknowledged. We acknowledge all project collaborators, including Estonian Land Board, Leica Geosystems, University of Joensuu, University of Helsinki, and the Finnish Geodetic Institute, and many persons whose hard work made this campaign possible. Especially Timo Tokola, Peep Krusberg, Teemu Hakala, Leena Matikainen and Juha Suomalainen are gratefully acknowledged. We also thank Gerrit de Leeuw for his efforts in establishing and maintaining the Hyytiälä AERONET-site and Janne Levula for providing the SMEAR-II data.